Optimal Control of an Energy-Recycling Actuator for Mobile Robotics Applications

Erez Krimsky and Steven H. Collins*

Abstract— Actuator power consumption is a limiting factor in mobile robot design. In this paper we introduce the concept of an energy-recycling actuator, which uses an array of springs and clutches to capture and return elastic energy in parallel with an electric motor. Engaging and disengaging clutches appropriately could reduce electrical energy consumption without sacrificing controllability, but presents a challenging control problem. We formulated the optimal control objective of minimizing actuator power consumption as a mixed-integer quadratic program (MIQP) and solved for the global minimum. For a given actuator design and a wide range of simulated torque and rotation patterns, all corresponding to zero net work over one cycle, we compared optimized actuator energy consumption to that of an optimized gear motor with simple parallel elasticity. The simulated energy-recycling actuator consumed less electrical energy: 57% less on average and 80% less in the best case. These results demonstrate an effective approach to optimal control of this type of system, and suggest that energy-recycling actuators could substantially reduce power consumption in some robotics applications.

Index Terms— Optimization and optimal control, force control, prosthetics and exoskeletons

I. INTRODUCTION

Many useful robotic tasks require performing almost no net positive mechanical work on their environments. These low net work tasks include a diverse range of behaviors such as robotic locomotion [1], pick-and-place [2], and in some cases lower limb prosthesis [3] and exoskeleton [4] assistance. Although these tasks do not inherently require large amounts of energy input, mobile robotic actuator inefficiency often leads to short run times and large batteries.

A. Electric Motors

Electric motors provide the versatility and controllability required to perform a wide range of tasks, but this performance comes at the cost of poor system efficiency. As motors are inefficient at low velocities, efficiency can typically be improved by employing a high gear reduction. However, high gear ratios lead to an increase in weight and inertia and often substantial losses due to gear friction. Additionally, high gear ratios can create non-backdrivable transmissions, which preclude the option of regenerative braking and can complicate torque sensing [5]. Research focusing on efficient actuation for quadrupedal locomotion has shown promising results by designing with a large motor radius, low gear ratio, well-tuned series stiffness, and efficient drive electronics [6].

However, ohmic losses inherent to electromagnetic actuation leave significant room for improvement.

B. Parallel Elastic Elements

Placing elastic elements in parallel with a robotic joint allows for passively generating torques at no additional power consumption costs. When placed in parallel with a motor on the same joint, this configuration is referred to as a parallel elastic actuator. When designing actuation for a specific task, the spring characteristics can be tailored such that the elastic element offloads the torque requirements of the motor [7]. This allows for lighter, lower-power motors, and often lower gear ratios which can reduce gearbox mass and losses [8]. Parallel elastic elements can also be used to passively shift the equilibrium point of a robotic joint, which can be especially useful in reducing power consumption for serial link robots that need to support their weight under gravity [9]. A downside of parallel elasticity is increased motor torque requirements when countering the elastic torques [8]; elasticity that is useful for one task may be detrimental for another. For example, the parallel elastic stiffness at a hip joint that is useful for walking on level ground would be detrimental for stair climbing, which requires a different neutral joint position.

C. Clutches

Whereas motors typically require high power consumption to produce static torques [10], active mechanical clutches have the potential to operate under high torques at a fraction of the power consumption [3]. Clutches can also improve parallel elastic actuator efficiency and robustness by only engaging elastic components when it is beneficial [7] [11]. However, in many cases clutch power consumption is still significant, and the additional energy cost of transporting added clutch mass can offset the energy savings provided. Devices with conventional clutch and spring elements have demonstrated capture and return of system kinetic energy with the goal of reducing actuator power consumption [8] [11]. However, as these systems only consist of a single spring, active clutch control can only dictate when a spring is engaged but not the corresponding spring torque.

To avoid the power consumption costs of active clutches, many devices have been designed with passive clutches. Passive mechanical clutches can be designed to engage or disengage at certain angles [4], or velocities [12] or engage upon the application of motor torques [13]. Passive clutches can also reduce power consumption by disengaging drive components and allowing outputs to swing freely according

to the passive system dynamics [13]. However, as with other passive devices, the power savings of passive clutches comes at the cost of versatility.

Electroadhesive clutches are an emerging technology that can combine the controllability of conventional active clutches with the low energy consumption of passive clutches. They have up to $\sim 10\times$ improvements in weight and $\sim 1000\times$ improvements in power consumption per unit force compared to conventional electromagnetic or magnetorheological clutches [14], and can be engaged or disengaged in under 30 ms [15]. Electroadhesive clutches consist of two thin, flexible electrodes with a large overlap area that can slide freely past each other when disengaged but adhere and resist shear forces when a high voltage is applied [16]. Although electroadhesive clutches require high voltages, they exhibit very low power consumption [15]. These clutches are lightweight, thin, and planar, so each clutch can be connected in series with a planar spring and multiple clutched-springs can be stacked in parallel for discrete stiffness selection. Highly efficient and lightweight active stiffness control enables exciting new design possibilities for robotic actuation.

II. ENERGY-RECYCLING ACTUATOR

A. Actuator Concept

The energy-recycling actuator consists of a parallel array of springs, each connected to two clutches. This allows each spring to be either engaged to a base frame and held in place, thereby maintaining its elastic energy, or connected to an output, thereby applying a force to its environment. By using multiple clutched springs in parallel, all connected to the same output, we can achieve discrete force control. To keep mass and power requirements low, planar natural rubber tension springs can be used for energy storage and electroadhesive clutches can be used for control. This is conceptualized with a side view of a single spring in Fig. 1.
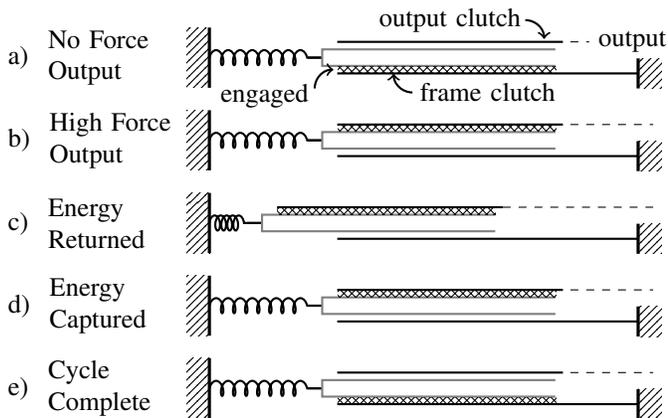

Fig. 1. Cross hatching shows engagement between clutch electrode pairs. Spring electrodes are shown in gray. (a) The spring is engaged to the frame and held in place while the output moves freely. (b) The spring force is transmitted to the output. (c) The spring has contracted and performed positive work. (d) The spring has extended and performed negative work. (e) The spring returns to its initial energy and clutch state.
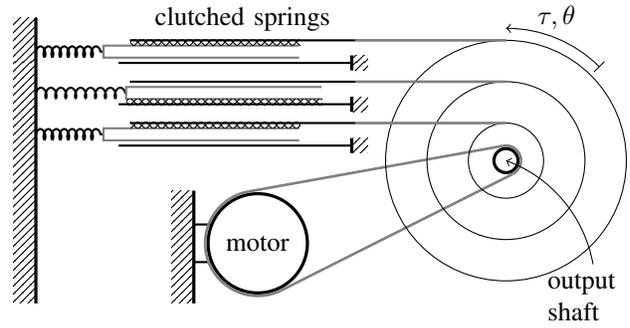

Fig. 2. One rotary configuration for an energy-recycling actuator, with each clutched spring and the motor connected to the same output shaft. At this instant, two springs are engaged to the output.

The principle of operation of an energy-recycling actuator is illustrated by a scenario in which the springs act on a pulley to raise and lower a mass against gravity. Engaging all the springs to the output will cause the mass to accelerate upward, gaining kinetic and gravitational potential energy, while the springs lose equivalent elastic energy. Disengaging some of the springs from the output will cause the mass to accelerate downward. By engaging more springs we may slow the descent and transfer the potential and kinetic energy of the mass into elastic energy in the actuator. At all times the total system mechanical energy remains constant.

Even for true zero net work tasks like moving a mass cyclically under gravity, elastic losses and friction will lead to a reduction in stored energy. To make up for these losses, we can add a motor in parallel with the springs. The motor allows the actuator to perform positive work and improves torque tracking resolution; the clutches can only be controlled discretely, whereas motor torque can be controlled continuously. Because the springs in the actuator are largely responsible for torque generation, the peak torque and peak mechanical power requirements for the motor in the actuator can be significantly lower than for the actuator itself. One possible actuator configuration is shown in Fig. 2. In this rotary configuration all of the springs and the motor apply torques about the same output shaft. Bidirectional torques could be achieved with a similar design by placing clutched springs on opposing sides of the output shaft. In some cases, such as ankle exoskeleton assistance, unidirectional torque is sufficient [16].

III. ENERGY-RECYCLING OPTIMAL CONTROL PROBLEM

A. Control Problem Formulation

In this section we pose actuator control optimization as a torque control problem, where the actuator tracks a predefined reference torque τ_{ref} while acting on a system whose displacements are assumed. This approach can be used for offline optimization of arbitrary scenarios, provided that the target torques and displacements are dynamically consistent.

We consider an actuator with n springs and a discrete-time control scheme with $N+1$ time points in the planning horizon. At time t^i, the control inputs for the actuator are

the binary clutch control vector $u^i \in \{0,1\}^n$, and the commanded motor current $I_m^i \in \mathbf{R}$. We will use $u_j^i = 1$ to denote that the jth spring is engaged to the output, and $u_j^i = 0$ to denote that the jth spring is engaged to the base frame. The state vector $x \in \mathbf{R}^n$ gives the position of the springs in the actuator. As the displacements are assumed to follow a reference trajectory, the state vector does not include the output position or velocity.

1) Torque Output: The total torque output from the actuator is the sum of the spring and motor torques given by

$$\tau_{\text{out}} = \tau_s + \tau_m. \tag{1}$$

Natural rubber elastomer springs follow a non-linear force-displacement relation [16]. To simplify the spring model, we linearized the spring force over a specified displacement range. With this linearization, the torque generated by an individual spring can be given as

$$\tau_{s,j} = r_j \left(b_j + k_j x_j \right), \tag{2}$$

where r_j is the pulley radius for the jth spring, b_j is the baseline force that the spring will exert at $x_j = 0$, and k_j is the linearized stiffness. We define $b, k, r \in \mathbf{R}^n$ for the baseline force, linearized stiffness, and pulley radius of the springs respectively. We also define a stiffness matrix K and a radius matrix R with k and r on their respective diagonals. The total spring torque exerted on the output is then given by

$$\tau_s = (b + Kx)^T Ru. \tag{3}$$

We consider the torques required to compensate for the inertia of the motor and gearbox leading to a total motor output torque given by

$$\tau_m = \tau_{em} - J_e \dot{\omega}, \tag{4}$$

where τ_{em} is the electromechanical contribution to gearbox output torque and J_e is the effective motor-gearbox inertia as seen by the output shaft. We consider a motor-gearbox model which accounts for energy losses by assuming motor Coulomb friction and fixed gearbox efficiency. Motor friction, which always opposes motor motion, is given as

$$\tau_f = -k_t I_{NL} \cdot \text{sign}\left(\omega\right), \tag{5}$$

where k_t is the motor torque constant and I_{NL} is the motor no-load current. The sign of the gearbox losses depends on whether the motor is driving the system output or being driven by it [17], leading to the switched equation

$$\tau_{em} = \begin{cases} \alpha\eta\left(k_t I_m + \tau_f\right) & I_m \cdot \text{sign}\left(\omega\right) \geq I_{NL} \\ \alpha\frac{1}{\eta}\left(k_t I_m + \tau_f\right) & I_m \cdot \text{sign}\left(\omega\right) < I_{NL}, \end{cases} \tag{6}$$

where η is the gearbox efficiency and α is the gear ratio.

2) System Dynamics and Constraints: The springs that are clutched to the base frame maintain their positions, while the springs that are clutched to the output will move. This gives the discrete time state update equation

$$x^{i+1} = x^i - \Delta\theta^i Ru^i, \tag{7}$$

where $\Delta\theta^i$ is the output displacement from t^i to t^{i+1}.

Due to the finite stiffness of the electrodes, the springs also move at the instant when clutch control is changed; the newly-engaged electrodes stretch, transferring elastic energy from the spring to the clutch and causing the spring to relax slightly. Denoting the clutch stiffness as k_c, the spring displacement before relaxation as x_j^{i-1}, and the spring relaxation distance as d_j, force equilibrium is reached when

$$b_j + k_j \left(x_j^{i-1} - d_j \right) = k_c d_j. \tag{8}$$

The clutch transition dynamics that occur when the clutch control vector is changed are then given by

$$x_j^i = x_j^{i-1} + d_j \left(2u_j^i u_j^{i-1} - u_j^i - u_j^{i-1} \right). \tag{9}$$

Here we use an electrode stiffness of 24 kN·m^{-1} based on experiments with similarly sized electrodes [14].

In addition to the equality constraints on the dynamics, we enforce an equality constraint on the output torque of the actuator given by

$$\tau_{\text{out}}^i = \tau_{\text{ref}}^i. \tag{10}$$

To ensure perfect torque tracking at the instant when the clutch control is changed, we allow motor current, and thereby torque, to change instantaneously to account for the spring torque before and after the clutch transition.

To prevent exceeding the voltage capabilities of the motor driver or overheating the motor we add two inequality constraints on the commanded current. Here we ignore the effects of motor inductance and assume the drive voltage v can be related to the motor current by

$$v^i = I_m^i R_m + k_e \alpha \omega^i \tag{11}$$

where R_m is the winding resistance and k_e is the speed constant ($k_e = k_t$). We assume a maximum drive voltage of ± 56 V and constrain the voltages to be within this range.

The motor nominal current I_{nom} dictates the continuous thermal power dissipation that can be achieved without damaging the motor. To prevent overheating the motor, we add a constraint that the integral of the Joule heating over the planning horizon is less than the maximum allowable thermal power dissipation, given by

$$\sum_{i=0}^{N-1} \frac{t^{i+1} - t^i}{2} (I_m^i)^2 R_m \leq \sum_{i=0}^{N-1} \frac{t^{i+1} - t^i}{2} I_{\text{nom}}^2 R_m, \tag{12}$$

where we use trapezoidal integration instead of simple summation to account for the discontinuities in motor current at clutch transitions.

3) Cost Function: The total power consumption of the actuator includes power consumption from the motor and the electroadhesive clutches. Here we ignore power losses from the motor driver electronics and assume the power consumed by the motor at time t^i is the product of the current and drive voltage given by

$$c_m^i = I_m^i \left(I_m^i R_m + k_e \alpha \omega^i \right). \tag{13}$$

Assuming a clutch capacitance of 20 nF and an operating voltage of 300 V the estimated energy consumption per

clutch change is $\frac{1}{2}cv^2 \approx 0.9$ mJ, which we will denote e_c. Here we ignore the clutch leakage currents, which will only contribute losses of ≈ 1 mW per spring [15]. The energy consumption with each clutch transition is then given by

$$c_c^i = e_c \sum_{j=1}^{n} \left(u_j^i - u_j^{i-1} \right)^2. \tag{14}$$

To prevent the springs from drifting over time and reaching their displacement limits, we add a terminal state cost on the spring positions given by

$$c_p = \rho \left\| x^N - x_{\text{nom}} \right\|^2, \tag{15}$$

where x^N is the terminal state, $x_{\text{nom}} = \frac{1}{2}x_{\text{max}}$ gives the midpoints of the allowable spring displacement ranges, and ρ is a weighting factor.

The total optimization problem is now given as

$$
\begin{aligned}
\underset{x^i, u^i \forall i}{\text{minimize}} \quad & \sum_{i=0}^{N-1} \left[\frac{t^{i+1} - t^i}{2} \left(c_m^i + c_m^{i+1} \right) + c_c^i \right] + c_p \quad (16) \\
\text{subject to} \quad & \text{Eq. 7, Eq. 9} \qquad \text{(dynamics constraints)} \\
& \mathbf{0} \preceq x^i \preceq x_{\text{max}} \,\forall i \quad \text{(state constraints)} \\
& \left. \begin{array}{l} u^i \in \{0,1\}^n \,\forall i \\ v_{\text{min}} \leq v^i \leq v_{\text{max}} \,\forall i \\ \text{Eq. 10, Eq. 12} \end{array} \right\} \text{(control constraints)}.
\end{aligned}
$$

B. Mixed-Integer Quadratic Programming

Minimizing (16) requires finding the optimal assignment of binary variables which leads to an optimization that is combinatorial in nature. Although there are a finite number of possible binary assignments, a brute force approach is intractable even for small problems.

We produce globally optimal solutions for the optimization problem (16) by formulating it as a mixed-integer quadratic program (MIQP). Any mixed-integer quadratic program can be written as

$$
\begin{aligned}
\underset{y}{\text{minimize}} \quad & y^T Q y + q^T y + c \\
\text{subject to} \quad & A_1 y = b_1 \\
& A_2 y \preceq b_2 \tag{17} \\
& y_i \in \{0,1\} \,\forall i \in \mathcal{B} \\
& y_{\text{min}} \preceq y \preceq y_{\text{max}},
\end{aligned}
$$

where y is the vector of optimization variables, $Q \succeq 0$ is the quadratic objective matrix, q is a linear objective term, and c is a constant. The matrices A_1 and A_2 are linear equality and inequality constraint matrices, and $\mathcal{B}$ is the set of indices in y that must take on binary values. If there are no binary constraints this problem is known as a quadratic program (QP). Quadratic programs are convex and can be solved efficiently [18]. However, restricting certain variables to the non-convex set of binary values makes the problem non-convex and NP-hard [19]. Nevertheless, many efficient algorithms for solving MIQPs have been developed.

The standard approach to constructing an optimization problem as an MIQP is to define a vector of optimization variables, write out the objective as a quadratic function of the optimization vector, and write the constraints as rows in the equality and inequality constraint matrices.

In our case, defining y to contain the state and control variables from every step, we find the objective function cannot be expressed as a quadratic function of y and the constraints cannot be constructed directly though linear equality and inequality constraints on y. To use an MIQP approach, we must first transform (16) into an equivalent problem of the form (17) by introducing new auxiliary optimization variables and constraints, allowing us to write the torque output and dynamics with linear expressions.

We start the process of transforming the torque output into a linear function of optimization variables by introducing the new optimization variable z_j^i which we would like to be equal to $x_j^i u_j^i$. This new variable allows us to write the spring torque (3) as a linear function of u^i and z^i given by

$$\tau_s^i = b^T R u^i + k^T R z^i. \tag{18}$$

Because $z_j^i = x_j^i u_j^i$ is a non-linear constraint, which is incompatible with (17), we instead introduce this equivalence by adding new inequalities that indirectly enforce the constraint. Defining a new variable, in our case z, which must be equivalent to the product of a binary variable and a continuous variable, in our case u and x respectively, can be accomplished by introducing the following four linear inequalities (see [20] equation 5b)

$$z_j^i \leq x_{j,\text{max}}^i u_j^i \tag{19a}$$
$$z_j^i \geq x_{j,\text{min}}^i u_j^i \tag{19b}$$
$$z_j^i \leq x_j^i - x_{j,\text{min}}^i (1 - u_j^i) \tag{19c}$$
$$z_j^i \geq x_j^i - x_{j,\text{max}}^i (1 - u_j^i), \tag{19d}$$

where $x_{j,\text{min}}^i$ and $x_{j,\text{max}}^i$ represent bounds on x_j^i. Although all these inequalities are linear, the only feasible solution results in $z_j^i \equiv x_j^i u_j^i$. To incorporate z into the MIQP, we add z to the optimization vector and we add these inequalities as rows in the inequality constraint matrix.

Writing the electromechanical torque as a linear function of optimization variables requires the introduction of the binary variable δ at each time step. We let $\delta = 1$ denote that the motor is driving the load, and let $\delta = 0$ denote that it is being driven, leading to

$$\tau_{em} = \alpha k_t \left(\delta \eta + \frac{1 - \delta}{\eta} \right) \left(I_m - I_{NL} \cdot \text{sign}\left(\omega \right) \right). \tag{20}$$

We also introduce the new optimization variable γ and add inequalities to enforce $\gamma^i \equiv \delta^i I_m^i$ following the same process for the product of continuous and binary variables as in (19). This lets us rewrite the electromechanical torque (20) as a linear function of optimization variables given by

$$\tau_{em} = \alpha k_t \left[\gamma \left(\eta - \frac{1}{\eta} \right) + \frac{1}{\eta} I_m \right.$$
$$\left. - \left(\frac{1 - \delta}{\eta} + \delta \eta \right) I_{NL} \cdot \text{sign}\left(\omega \right) \right]. \tag{21}$$

The last step in writing the torque as a linear function of optimization variables is to introduce inequalities that enforce proper assignment of δ at each time step. Relating a binary variable to the truth value of a linear inequality can be accomplished by enforcing two inequalities (see [20] equation 4e). From (6) we require $[\delta^i = 1] \iff [I_{NL} - I_m^i \text{sign}(\omega^i) \leq 0]$. Letting $\psi(I_m^i) = I_{NL} - I_m^i \text{sign}(\omega^i)$, we find that δ will be assigned correctly by adding the following linear inequalities into our inequality constraint matrix

$$\psi(I_m^i) \leq \psi_{\max}\left(1 - \delta^i\right) \tag{22a}$$

$$\psi(I_m^i) \geq \varepsilon + (\psi_{\min} - \varepsilon)\delta^i, \tag{22b}$$

where $\psi_{\min}, \psi_{\max}$ are lower and upper bounds on ψ, and ε is a small number, often the machine precision.

In addition to expressing the torque output as a linear function of optimization variables, we also need to express the dynamics constraints using only linear equalities or inequalities of optimization variables. The expression for elastic losses in the dynamics (9) is non-linear and requires the introduction of new variables and constraints. We first introduce a binary variable $g_j^i \equiv u_j^i u_j^{i-1}$. As g_j^i is the product of two binary variables we can use just three inequality constraints to enforce equivalence (see [20] equation 5a). We also introduce continuous variables $p_j^i \equiv x_j^{i-1} g_j^i$ and $a_j^i \equiv x_j^{i-1} u_j^i$. As these are products of continuous and binary variables we can use the process of (19) to incorporate these variables into the MIQP by adding inequalities. This allows us to rewrite (9) as a linear equality given by

$$x_j^i = x_j^{i-1} + \left(\frac{b_j}{k_c + k_j}\right)\left(2g_j^i - u_j^i - u_j^{i-1}\right) + \left(\frac{k_j}{k_c + k_j}\right)\left(2p_j^i - a_j^i - z_j^{i-1}\right). \tag{23}$$

When the motor is doing negative work, using (13) to model the power consumption will often overestimate the benefits of regenerative braking. To ignore regeneration, we can constrain motor power consumption to be non-negative by letting c_m^i be an optimization variable which should be equivalent to $\max\{I_m^i\left(I_m^i R_m + k_e \alpha \omega^i\right), 0\}$. This is done by adding the following constraints

$$c_m^i \geq 0 \tag{24a}$$

$$c_m^i \geq I_m^i\left(I_m^i R_m + k_e \alpha \omega^i\right). \tag{24b}$$

These inequalities and the inequality constraint on Joule heating convert the optimization problem from a standard form MIQP to a mixed-integer quadratically-constrained quadratic program (MIQCQP). Although often more computationally demanding than standard MIQPs, large MIQCQPs have been solved in real time for robotic locomotion tasks [21].

IV. SIMULATIONS

A. Test Cases

To compare energy-recycling actuator performance to a conventional motor-gearbox system without biasing the design towards a specific task, we generated 100 random cyclic torque and velocity test profiles that result in zero net work.

Each test profile satisfies $\int_0^T \tau_{\text{ref}}(t)\omega(t)\, dt = 0$, where T is the cycle period. For each profile the maximum absolute position was in the range of $30°$ to $40°$, with a minimum change of $30°$ over the cycle. The peak torque was 30 N·m and the minimum torque was between 0 and 30 N·m.

B. Optimal Motor Selection

To make a fair comparison between the energy-recycling actuator and a conventional motor and gearbox with parallel elasticity, we first ran an optimization to find the motor-gearbox parallel-elastic configuration that gave the lowest average cost over the test profiles using the motor-gearbox model described above. To select a motor we ran a brute force optimization on motor and gearbox parameters from the Maxon-Motor online catalog [22] (data available at [23]). For a given set of motor parameters, the total output torque can be written as a linear function of the drive current and the parallel-elastic spring parameters, allowing us to generate one large mixed-integer quadratic program that includes all of the test profiles and optimize the parallel-elastic parameters and the control simultaneously for each candidate motor. We ran two optimizations to account for scenarios with and without regenerative braking. We found Maxon motor 578298, gearbox 223091, and motor 634043, gearbox 223087, to be optimal for the cases with and without regeneration, respectively.

C. Actuator Parameters

For the simulations presented here we used $n = 5$ springs as this struck a good balance between actuator performance and computational complexity. We considered an actuator with a length of 55 cm, width of 15 cm, and maximum output shaft pulley radius 11.5 cm. For each spring we used experimentally determined material constants from [14]. The spring displacement ranges were selected so that each spring could always be engaged to the frame or the output for $0 \leq x \leq x_{\max}$ (assuming a clutch holding force per overlap area of 7800 N·m^{-2}). We used the same motor for the energy-recycling actuator as for the simple parallel elastic configuration but used a slightly lower gear ratio because this improved performance (with regeneration: Maxon gearbox 223089, without regeneration: gearbox 223086).

D. Simulation Settings

For all simulations we used a cycle time of $T = 1$ second, a clutch control frequency of 10 Hz, and a motor control frequency of 40 Hz. The clutches are controlled at a lower frequency due to limits on their engage and release times. We used the commercial solver Gurobi to generate solutions [24].

For each torque-displacement profile, we optimized the actuator control for 10 cycles using a receding horizon control approach. Each trajectory begins with $x^0 = x_{\text{nom}}$ and all clutches engaged to the frame. To generate a trajectory, we optimize the control for the upcoming 1.1 cycles and execute the first 0.1 seconds of the plan, corresponding to one change of the clutch control vector. After updating the clutch control, we reoptimize for the following 1.1 cycles

using the result of the previous optimization to warm start the solution and improve the solve time. In the following section we report values from the last of the 10 cycles.

The computations were run on a desktop computer with an Intel i7-8700 3.20 GHz processor with 6 cores. All results reported here are within 0.1% of the true optimal values.

V. RESULTS

The energy-recycling actuator used significantly less energy than the motor with optimized parallel elasticity. The average reduction in electrical energy consumption over all the profiles tested was 57% (50% with regeneration), with a maximum reduction of 80% (86% with regeneration). The data from the last cycle for the profile with the largest percent reduction are shown in Fig. 3. The energy-recycling actuator resulted in lower energy consumption for all 100 test profiles.

The energy-recycling actuator required lower peak motor torque than the motor with a parallel spring, on average. The mean peak electromechanical torque for the motor in the actuator was 12.6 ± 2.3 (13.4 ± 2.6 with regeneration) N·m whereas the mean peak torque from the motor with a parallel spring was 18.7 ± 0.7 (18.8 ± 3.2 with regeneration) N·m.

The computation time for the initial control step was 16.3 ± 16.6 seconds. For all subsequent steps the average computation time was 4.8 ± 4.7 seconds, where the increase in speed is due to warm starting the solver with the solution from the previous step.

VI. DISCUSSION AND FUTURE WORK

We found that an optimally controlled energy-recycling actuator can halve electrical power consumption in some tasks. For mobile robots or exoskeletons, this could substantially reduce battery mass or increase operating time. Reduced peak motor torque requirements might also allow for smaller motors and gears with less mass.

A variety of simplifying assumptions have been made for the actuator model to make the control scheme tractable. In this work we used a simple linear spring model for the elastomer spring. If this linearization proves too coarse, a piecewise affine approximation could be used at the cost of increased computational complexity. Here we also ignore potential hysteresis resulting from viscoelastic spring properties. Although any elastomeric material will have some hysteresis, natural rubbers exhibit significantly lower hysteretic energy loss than most elastomers [25].

Our model also makes some simplifying assumptions about the system dynamics when the clutch control is changed by assuming that clutch states and motor current can change instantaneously. In our intended robotic and exoskeleton applications, the energy-recycling actuator will be interacting with substantial inertia. As such, transients in the torque production on the order of 50 ms are not expected to significantly affect the resulting trajectories. External disturbances and model errors will eventually cause the joint trajectory to drift from the initial reference. This drift will be compensated for by periodically replanning new dynamically consistent trajectories.

It is unlikely that the MIQP formulation for (16) can be solved to optimality with the restrictions imposed by real time control for mobile robots. A simple solution to this problem is to set a time limit on the solver and return the best feasible solution found within the allowable computation time. Another approach is to use algorithms that approximately solve MIQPs [19], which may sacrifice optimality guarantees but can produce usable solutions very quickly.

VII. CONCLUSIONS

Here we have presented the concept of an energy-recycling actuator to reduce electrical energy consumption in robotic systems. We have shown how optimal control of the energy-recycling actuator can be solved by constructing the problem as a mixed-integer quadratic program. We have presented simulations comparing the energy-recycling actuator to a standard motor with parallel elasticity, each under optimal control, under a wide range of test trajectories with zero net work. We found that the energy-recycling actuator reduced power consumption by a factor of two on average and five at best. These promising simulation results motivate future design optimization and hardware implementation.
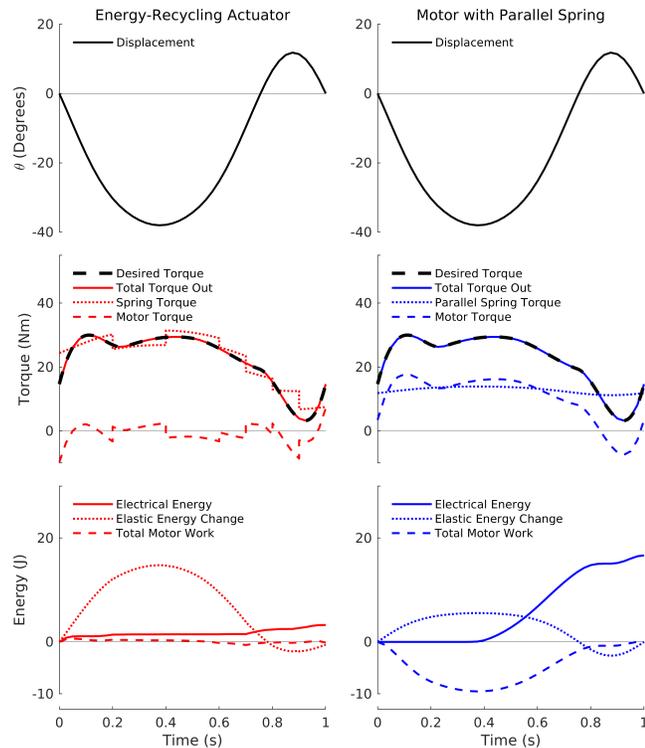
ACKNOWLEDGMENT

Fig. 3. Best case percent energy reduction for the no-regeneration case. The springs in the energy-recycling actuator provide most of the required torque and the contributions from the motor are small.

REFERENCES

[1] S. Collins, A. Ruina, R. Tedrake, and M. Wisse, "Efficient Bipedal Robots Based on Passive-Dynamic Walkers," *Science*, vol. 307, no. 5712, pp. 1082–5, Feb. 2005.

[2] L. F. v. d. Spaa, W. J. Wolfslag, and M. Wisse, "Unparameterized Optimization of the Spring Characteristic of Parallel Elastic Actuators," *IEEE Robotics and Automation Letters*, vol. 4, no. 2, pp. 854–861, Apr. 2019.

[3] E. J. Rouse, L. M. Mooney, and H. M. Herr, "Clutchable series-elastic actuator: Implications for prosthetic knee design," *The International Journal of Robotics Research*, vol. 33, no. 13, pp. 1611–1625, Nov. 2014.

[4] S. H. Collins, M. B. Wiggin, and G. S. Sawicki, "Reducing the energy cost of human walking using an unpowered exoskeleton," *Nature*, vol. 522, no. 7555, pp. 212–215, June 2015.

[5] S. Seok, A. Wang, D. Otten, and S. Kim, "Actuator design for high force proprioceptive control in fast legged locomotion," in *2012 IEEE/RSJ International Conference on Intelligent Robots and Systems*, Oct. 2012, pp. 1970–1975.

[6] S. Seok, A. Wang, M. Y. Chuah, D. J. Hyun, J. Lee, D. M. Otten, J. H. Lang, and S. Kim, "Design Principles for Energy-Efficient Legged Locomotion and Implementation on the MIT Cheetah Robot," *IEEE/ASME Transactions on Mechatronics*, vol. 20, no. 3, pp. 1117–1129, June 2015.

[7] M. Plooij, W. Wolfslag, and M. Wisse, "Clutched Elastic Actuators," *IEEE/ASME Transactions on Mechatronics*, vol. 22, no. 2, pp. 739–750, Apr. 2017.

[8] M. Plooij, M. v. Nunspeet, M. Wisse, and H. Vallery, "Design and evaluation of the Bi-directional Clutched Parallel Elastic Actuator (BIC-PEA)," in *2015 IEEE International Conference on Robotics and Automation (ICRA)*, May 2015, pp. 1002–1009.

[9] Z. Ren, W. Roozing, and N. G. Tsagarakis, "The eLeg: A Novel Efficient Leg Prototype Powered by Adjustable Parallel Compliant Actuation Principles," in *2018 IEEE-RAS 18th International Conference on Humanoid Robots (Humanoids)*, Nov. 2018, pp. 1–9.

[10] M. Plooij, G. Mathijssen, P. Cherelle, D. Lefeber, and B. Vanderborght, "Lock Your Robot: A Review of Locking Devices in Robotics," *IEEE Robotics Automation Magazine*, vol. 22, no. 1, pp. 106–117, Mar. 2015.

[11] B. Penzlin, M. E. Fincan, Y. Li, L. Ji, S. Leonhardt, and C. Ngo, "Design and Analysis of a Clutched Parallel Elastic Actuator," *Actuators*, vol. 8, no. 3, p. 67, Sept. 2019.

[12] D. Shin, A. Tanaka, N. Kim, and O. Khatib, "A Centrifugal Force-Based Configuration-Independent High-Torque-Density Passive Brake for Human-Friendly Robots," *IEEE/ASME Transactions on Mechatronics*, vol. 21, no. 6, pp. 2827–2835, Dec. 2016.

[13] M. Hild, T. Siedel, and T. Geppert, "Design of a Passive, Bidirectional Overrunning Clutch for Rotary Joints of Autonomous Robots," in *Intelligent Robotics and Applications*, ser. Lecture Notes in Computer Science, S. Jeschke, H. Liu, and D. Schilberg, Eds. Springer Berlin Heidelberg, 2011, pp. 397–405.

[14] S. B. Diller, "Design, characterization, and implementation of lightweight and energy-efficient electroadhesive clutches for robotics," Ph.D. dissertation, Carnegie Mellon University, 2018.

[15] S. B. Diller, S. H. Collins, and C. Majidi, "The effects of electroadhesive clutch design parameters on performance characteristics," *Journal of Intelligent Material Systems and Structures*, vol. 29, no. 19, pp. 3804–3828, Nov. 2018.

[16] S. Diller, C. Majidi, and S. H. Collins, "A lightweight, low-power electroadhesive clutch and spring for exoskeleton actuation," in *2016 IEEE International Conference on Robotics and Automation (ICRA)*, May 2016, pp. 682–689.

[17] T. Verstraten, P. Beckerle, R. Furnémont, G. Mathijssen, B. Vanderborght, and D. Lefeber, "Series and Parallel Elastic Actuation: Impact of natural dynamics on power and energy consumption," *Mechanism and Machine Theory*, vol. 102, pp. 232–246, Aug. 2016.

[18] S. Boyd and L. Vandenberghe, *Convex Optimization*, 1st ed. Cambridge University Press, Mar. 2004.

[19] R. Takapoui, N. Moehle, S. Boyd, and A. Bemporad, "A simple effective heuristic for embedded mixed-integer quadratic programming," in *2016 American Control Conference (ACC)*, July 2016, pp. 5619–5625.

[20] A. Bemporad and M. Morari, "Control of systems integrating logic, dynamics, and constraints," *Automatica*, vol. 35, no. 3, pp. 407–427, Mar. 1999.

[21] R. Deits and R. Tedrake, "Footstep planning on uneven terrain with mixed-integer convex optimization," in *2014 IEEE-RAS International Conference on Humanoid Robots*, Nov. 2014, pp. 279–286.

[22] Maxon Motors. (2019). [Online]. Available: https://www.maxongroup.com/maxon/view/content/index

[23] [Online]. Available: https://github.com/ekrimsk/maxon_data

[24] Gurobi Optimization. (2019). [Online]. Available: https://www.gurobi.com/

[25] Z. Wang, C. Xiang, X. Yao, P. Le Floch, J. Mendez, and Z. Suo, "Stretchable materials of high toughness and low hysteresis," *Proceedings of the National Academy of Sciences*, vol. 116, no. 13, pp. 5967–5972, Mar. 2019.